Self-assembly of ordered wurtzite/rock salt heterostructures - a new view on phase separation in $Mg_xZn_{1-x}O$

K. I. Gries[1], T. A. Wassner[2], S. Vogel[1], J. Bruckbauer[2], I. Häusler[3], R. Straubinger[1], A. Beyer[1], A. Chernikov, B. Laumer[2,4], M. Kracht[4], C. Heiliger[4], J. Janek[5], S. Chatterjee[1], K. Volz[1], and M. Eickhoff[4]

[1]Faculty of Physics and Materials Sciences Center, Philipps-Universität Marburg, 35032 Marburg, Germany.

[2]Walter Schottky Institut, Technische Universität München, Am Coulombwall 4, 85748 Garching, Germany

[3]Institut für Physik, Humboldt-Universität zu Berlin, Newtonstraße 15, 12489 Berlin, Germany.

[4]I. Physikalisches Institut and Laboratorium für Materialforschung (LaMa), Justus-Liebig-Universität Gießen, Heinrich-Buff-Ring 16, 35392 Gießen, Germany, Germany.

[5] Institute for Physical Chemistry and Laboratorium für Materialforschung (LaMa), Justus-Liebig-Universität Gießen, Heinrich-Buff-Ring 58, 35392 Gießen, Germany, Germany.

The self-assembled formation of ordered, vertically stacked rocksalt/wurtzite $Mg_xZn_{1-x}O$ heterostructures by planar phase separation is shown. These heterostructures form quasi “natural” two-dimensional hetero-interfaces between the different phases upon annealing of MgO-oversaturated wurtzite $Mg_xZn_{1-x}O$ layers grown by plasma-assisted molecular beam epitaxy on c-plane sapphire substrates. The optical absorption spectra show a red shift simultaneous with the appearance of a cubic phase upon annealing at temperatures between 900°C and 1000°C. Transmission electron microscopy reveals that these effects are caused by phase separation leading to the formation of a vertically ordered rock salt/wurtzite heterostructures. To explain these observations we suggest a phase separation epitaxy model that considers this process being initiated by the formation of a cubic $(Mg,Zn)Al_2O_4$ spinel layer at the interface to the sapphire substrate, acting as a planar seed for the epitaxial precipitation of rock salt-type $Mg_xZn_{1-x}O$. The equilibrium fraction x of magnesium in the resulting wurtzite (rock salt) layers is approximately 0.15 (0.85), independent of the MgO content of the as-grown layer and determined by the annealing temperature. This model is confirmed by photoluminescence analysis of the resulting layer systems after different annealing temperatures. In addition we show that the thermal annealing process

results in a significant reduction in the density of edge- and screw-type dislocations, providing the possibility to fabricate high quality templates for quasi-homoepitaxial growth.

Introduction

The wurtzite-(wz-)ZnO/$Mg_xZn_{1-x}O$ material system holds several advantages for application in optoelectronic devices such as the high bulk exciton binding energy of 59 meV [1, 2] which increases beyond 100 meV in quantum structures [3-5]. Furthermore, the direct band gap extends from 3.3 eV to 4.5 eV when the Mg fraction x is increased up to 0.44 [6-8]. The similar ionic radii of Zn^{2+} (0.6 Å) and Mg^{2+} (0.57 Å) on tetrahedral lattice sites in wz-$Mg_xZn_{1-x}O$ lead to a small increase of the a-plane lattice parameter of only 3.6 x 10^{-5} per percent of incorporated MgO and hence allow the fabrication of quantum structures such as superlattices with low densities of structural defects [6, 9].

ZnO crystallizes in the wz-structure (lattice parameters a = 3.25 Å, c = 5.21 Å) while the thermodynamically stable phase of MgO is the cubic rock salt (rs-) structure (a = 4.21 Å) [10]. Hence, alloying of wz-ZnO with rs-MgO results in mixing of wz- and rs-phases once a critical MgO-concentration is exceeded. The thermodynamic solubility limit of MgO in $Mg_xZn_{1-x}O$ is less than 0.04 in bulk crystals [11]. Significantly higher values - of more than x = 0.40 - have been reported for thin films grown under non-equilibrium conditions [6-8, 12-14]. However, such wz-$Mg_xZn_{1-x}O$ films with high MgO-concentrations are metastable and thus thermal annealing affects their structural and optical properties as it can cause a separation of the rs- and wz-$Mg_xZn_{1-x}O$ phases on the way to equilibrium. The microscopic details of these widely recognized phase separation processes in the $Mg_xZn_{1-x}O$ system have only been sparsely addressed [7, 15-18] and phase separation is generally considered as a hardly controllable process which is responsible for the thermal instability of ternary compounds and results in the deterioration of the structural, optical, and electronic properties.

In this work we show that thermally induced phase separation in oversaturated wz-$Mg_xZn_{1-x}O$ grown on c-plane sapphire substrates by plasma-assisted molecular beam epitaxy (PAMBE) results in the formation of ordered vertical rs-/wz- $Mg_xZn_{1-x}O$ heterostructures with significantly reduced densities of edge- and screw dislocations compared to the initial layer. We show that the number of layers and their thickness are determined by the initial MgO-content x_0 while their composition depends on the

annealing temperature. The vertical phase separation process is initiated by the formation of a spinel layer with (111) orientation at the interface to the sapphire substrate, acting as a planar seed for the epitaxial precipitation of rs-$Mg_xZn_{1-x}O$. This phase separation epitaxy process results in the generation of novel heterostructures with natural hetero-interfaces and allows the fabrication of high quality rock salt and wurtzite $Mg_xZn_{1-x}O$ templates starting from a defective and metastable wurtzite $Mg_xZn_{1-x}O$ film.

Experimental details

Wurtzite- $Mg_xZn_{1-x}O$ layers with a thickness between 500 nm and 700 nm were grown on c-plane sapphire substrates by PAMBE at growth temperatures of 280°C applying the growth process described in ref. [8]. Growth was initiated by deposition of a MgO/ZnO double buffer layer realized by deposition of MgO film at 500°C and a ZnO layer at 300°C, followed by an annealing step at 600°C in vacuum [8,19]. Wurtzite $Mg_xZn_{1-x}O$ thin films were deposited at a substrate temperature of 280°C and a Zn beam equivalent pressure (BEP_{Zn}) of $6.1x10^{-5}$ mbar. Different Mg contents in the resulting wz-films were obtained by a variation of the BEP_{Mg} between 0 and $5.5x10^{-8}$ mbar. The MgO-fraction of the as-deposited wz-$Mg_xZn_{1-x}O$ layers in this study was determined to x_0 = 0, 0.05, 0.10, 0.20, 0.30, and 0.40 using optical transmission spectroscopy according to refs. [8,21].

Thermal annealing was performed for 60 min in a tube furnace in a constant oxygen flow of 0.4 SLPM (0.675 Pa m^3s^{-1}) at ambient pressure at annealing temperatures T_a between 800°C and 1000°C. Sample characterization before and after annealing was performed by optical transmission spectroscopy, transmission electron microscopy (TEM), high resolution X-ray diffraction (HRXRD), steady-state as well as time-resolved photoluminescence spectroscopy (PL, TRPL).

For HRXTD analysis a Phillips XPert MRD diffractometer equipped with a Bartels monochromator (Cu Kα line) was used. Low temperature optical transmission measurements were performed in a cold finger cryostat using a PerkinElmer UV/VIS/NR Lambda 900 spectrometer after backside polishing of

the sapphire substrates. Time-resolved PL experiments were performed using a 100 fs, 80 MHz repetition rate Ti:sapphire laser frequency-tripled to 4.3 eV for excitation. The sample was mounted inside a He-flow microscopy cryostat and the luminescence signal was collected in reflection geometry, dispersed in a monochromator and detected using a multichannel plate and CCD camera. All measurements were performed at T = 10 K with the excitation density of $6x10^{11}$ cm^{-2} photons per pulse.

Structural characterization was performed by transmission electron microscopy (TEM). Detection of diffraction patterns, weak beam dark field and bright field images were performed using a JEM 3010 (JEOL, Tokyo, Japan) microscope with a thermionic LaB6 cathode working at 300 kV. Scanning TEM (STEM) as well as energy dispersive X-ray (EDX) spectroscopy (detector: XFlash R 5000, Bruker, Ettlingen, Germany) was performed on an uncorrected and also on a double Cs corrected field emission gun TEM/STEM 2200FS (JEOL, Tokyo, Japan) working at 200kV. EDX spectra have been quantified using the software Esprit Version 1.9 (Bruker, Ettlingen, Germany). All STEM images have been recorded using a high angle annular dark field (HAADF) detector (JEOL, Tokyo, Japan). To determine the quantitative composition of the elements oxygen, aluminum, magnesium and zinc in the different samples by TEM-EDX the four Cliff-Lorimer factors had to be aligned. First, the factors were calibrated in the Al_2O_3 substrate which exhibits a well-defined composition. Afterwards, the factors have been aligned iteratively until the oxygen concentration in the $Mg_xZn_{1-x}O$ layers was 50 at%.

Analysis of threading dislocations: In the wurtzite structure three kinds of dislocations extended along the [0001]-direction exist: two variations of edge dislocations with burgers vectors $\vec{b}_1$ = 1/3 [-12-10] and $\vec{b}_2$= [-1100] and a screw dislocation with the burgers vector $\vec{b}_3$ = [0001] [22]. Using the weak beam (WB) dark field (DF) TEM imaging mode [23] edge dislocations are visible in (2-420) and (2-200) reflex images, while screw dislocations are highlighted in 000-4 WBDF images. In all cases the g-3g condition was used [24]. Due to the large lattice plane spacing in $Mg_xZn_{1-x}O$, i.e., a small reciprocal distance in the diffraction pattern, second order reflexes have been chosen for WBDF

imaging. In this work we only discuss samples oriented in the [10-10] zone axis of $Mg_xZn_{1-x}O$ and [2-200] WBDF images will not be presented.

Results

The effect of thermal annealing on the position of the fundamental absorption edge E_{opt} was analyzed by optical transmission measurements according to reference [8][20]. The resulting shift, ΔE_{opt}, is shown as a function of the annealing temperature in **Fig. 1**. No effect on E_{opt} was found for $x_0 \leq 0.10$. For $0.30 \geq x_0 \geq 0.20$ and annealing temperatures $T_a \leq 850°C$, a slight blue-shift is observed, while a red shift is found for $T_a > 850°C$. Both trends increase in magnitude with increasing x_0, the red shift also increases with increasing T_a. While a red-shift of 95 meV is found for $x_0 = 0.20$ annealed at 1000°C, ΔE_{opt} is determined to be –510 meV for $x_0 = 0.40$. Moreover, the observed shift in the optical absorption edge occurs at lower T_a when x_0 is increased

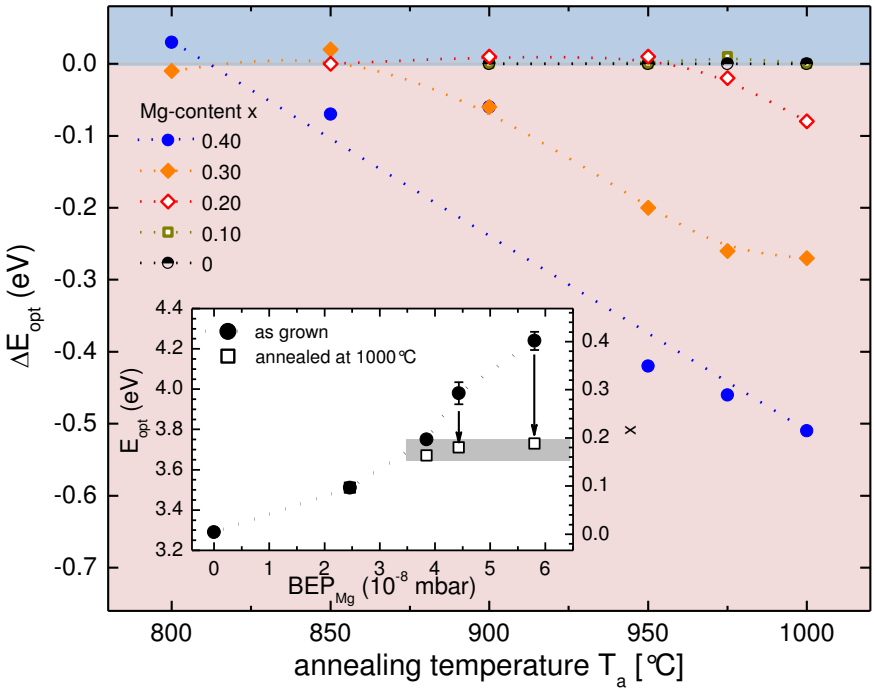

Fig. 1 Variation in the optical absorption edge as a function of the annealing temperature for different initial Mg-contents. For clarity the sample with $x_0 = 0.05$ is not displayed. The insert shows the variation of E_{opt} for the different wz-$Mg_xZn_{1-x}O$ samples upon annealing at T_a = 1000°C as a function of the Mg beam equivalent pressure (BEP_{Mg}) used during growth. The respective Mg-fractions extracted from optical absorption measurements are depicted on the right vertical axis.

The inset in **Fig. 1** shows that the optical absorption edge after annealing at T_a = 1000°C is determined to (3.70±0.05) eV for all the samples with $x_0 > 0.10$ within the experimental accuracy [20], corresponding to a Mg-fraction of (17±2)% [8,16]. This suggests that the position of E_{opt} after annealing is determined by the annealing temperature above a critical value for x_0.

In order to reveal structural changes we performed HRXRD measurements on the $Mg_{0.40}Zn_{0.60}O$ sample which showed the largest change in E_{opt}. In **Fig.2,** 2Θ-Ω-scans of the as-grown sample are compared to those obtained after annealing at different temperatures between 800°C and 1000°C. All spectra exhibit pronounced diffraction peaks related to the (00.2) wz-$Mg_xZn_{1-x}O$ reflex and the (00.6) reflex of the sapphire substrate. The broad signals at diffraction angles of 38.3° and 44.5° originate from the aluminum sample holder. Additionally, a reflex related to (111) rs-$Mg_xZn_{1-x}O$ is found for $T_a \geq$ 850°C and for T_a > 975°C a weaker reflex related to (002) rs-$Mg_xZn_{1-x}O$ is observed (grey shaded areas).

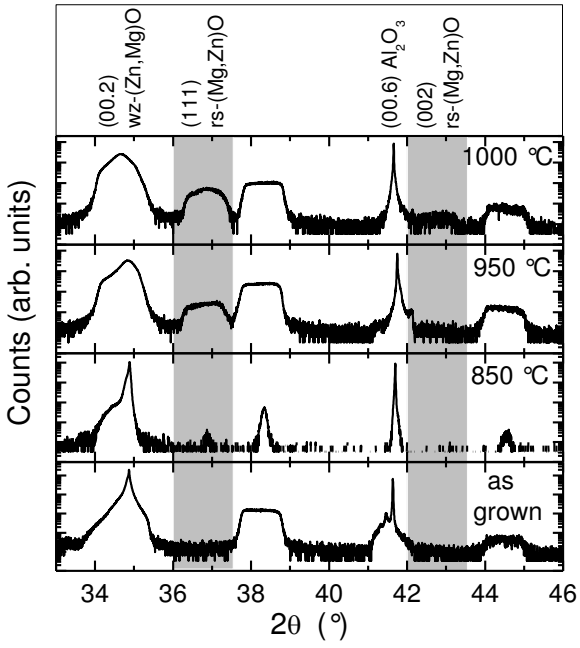

Figure 2 2Θ-Ω scans of $Mg_xZn_{1-x}O$ films with x_0= 0.40 after annealing at temperatures between 800 °C and 1000 °C (logarithmic scale). The regions of the (111) and (002) rs-$Mg_xZn_{1-x}O$-reflex are highlighted by the shaded area. Specimens annealed at 850 °C and above exhibit a clear (111) rs-$Mg_xZn_{1-x}O$-reflex. At higher annealing temperatures a weak signal of the (002) rs-$Mg_xZn_{1-x}O$-reflex is also observed. The broad signals at diffraction angles of 38.3° and 44.5° originate from the aluminum sample holder.

The cubic reflexes only appear for $x_0 \geq 0.20$ and above a critical annealing temperature that decreases with increasing x_0. This temperature is approximately 900°C for $x_0 = 0.30$ while only a weak (111) cubic $Mg_xZn_{1-x}O$ reflex is observed after annealing samples with $x_0 = 0.20$ at 975°C. These results indicate that a rs-phase with predominant (111)-orientation is formed upon annealing of wz-$Mg_xZn_{1-x}O$ thin films with $x_0 \geq 0.20$.

In contrast to this result, only the appearance of the (002) reflex of rs-$Mg_xZn_{1-x}O$ after annealing of wz-$Mg_xZn_{1-x}O$ films was reported for various growth techniques and substrates [7,15,16]. A comparison to those findings indicates that the presence of the MgO/ZnO buffer layer in combination with the c-plane sapphire substrate is the crucial factor for the preferential [111]-orientation of the rs-phase after annealing as observed in the present study.

The position 2Θ–diffraction angle for the (00.2) reflex form HRXRD measurements and the extracted c-lattice parameter as a function of E_{opt} after annealing at different T_a for the $Mg_{0.40}Zn_{0.60}O$-sample is compared to the respective values of as-grown wz-$Mg_xZn_{1-x}O$ films with different x_0 in **Figure 3**.

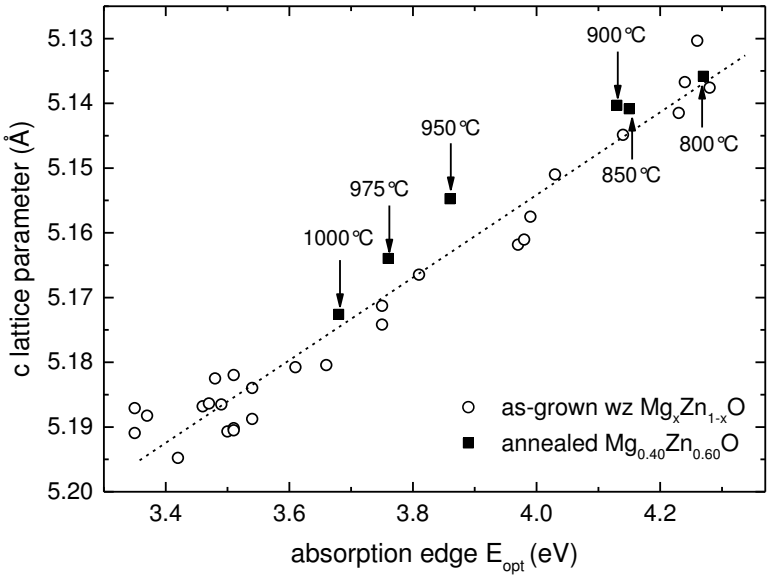

Figure 3 c-lattice parameter calculated from the position of the (00.2) reflection 2θ angle as a function of the absorption edge for as-grown wurtzite $Mg_xZn_{1-x}O$ films (open circles) in comparison to the annealed $Mg_{0.40}Zn_{0.60}O$ films (solid squares).

The agreement of both data sets demonstrates that the absorption properties of the $Mg_{0.40}Zn_{0.60}O$ layer after annealing at different temperatures are dominated by wz-$Mg_xZn_{1-x}O$ whose Mg-fraction decreases with increasing T_a. The appearance of an rs-phase with preferential (111) orientation and the simultaneous decrease of the Mg content in the wz-phase indicate a partial transformation from wz- to rs-material which is caused by a transfer of Mg^{2+}-ions from the wz- to the rs- phase.

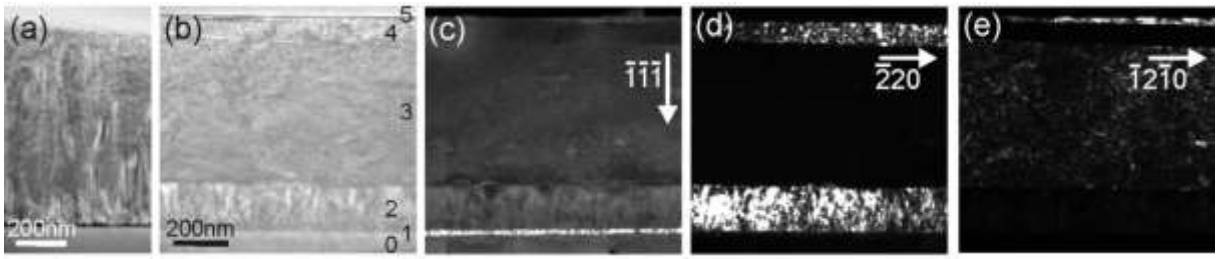

Figure 4 (a) TEM image along the [10-10] zone axis of the $Mg_{0.40}Zn_{0.60}O$ film grown on Al_2O_3 substrate and a MgO/ZnO-buffer layer. **(b)** TEM image of the $Mg_{0.40}Zn_{0.60}O$ film after annealing at 1000°C. The numbers enumerate the five distinct layers. **(c-e)** TEM dark field images with enhanced contrast. Depending on the chosen reflex different phases appear bright. (c) The spinel layer using the $(\bar{1}\bar{1}\bar{1})$ reflex of the spinel lattice; (d) the rs-$Mg_xZn_{1-x}O$ layers using the $(\bar{2}20)$ reflex of the rs-lattice; (e) the wz- $Mg_xZn_{1-x}O$ layers using the $(\bar{1}2\bar{1}0)$ reflex of the wz-lattice.

To study the microscopic characteristics of these effects we have analyzed the $Mg_{0.40}Zn_{0.60}O$ sample before and after annealing at 1000°C using TEM (**Fig.4**). **Figure 4a** presents a TEM image taken along the [10-10] zone axis of the as-grown $Mg_{0.40}Zn_{0.60}O$ sample. A homogeneous, defective wz-$Mg_xZn_{1-x}O$ film with a high density of threading dislocations and a thickness of 700 nm is visible. The MgO/ZnO-buffer layer is located between the wz-$Mg_xZn_{1-x}O$ layer and the Al_2O_3 substrate.

The TEM image of the same layer after annealing (1000°C, 1 h) in **Fig. 4b** reveals that the film has separated into five distinct layers identified by analysis of the respective electron diffraction pattern (supplemental **Fig.S1** [26]) [27]. TEM dark field images with enhanced contrast by choosing characteristic reflexes of the different phases were recorded to identify the different layers labeled by numbers in **Figs. 4c-e**. (1): a [111] spinel-$(Mg,Zn)Al_2O_4$ layer on top of the Al_2O_3 substrate; (2) and (4): [111]-oriented rs-$Mg_xZn_{1-x}O$ layers; (3) and (5): [0001]-oriented wz-$Mg_xZn_{1-x}O$ layers (rotated by 30° around the c-axis with respect to the Al_2O_3 substrate [8]). The crystal structure and epitaxial relation of the five layers with respect to the sapphire substrate are summarized in **Table 1.**

layer #	structure	composition	orientation			d (x=0.40)	d (x=0.30)
5	wz	$Mg_{0.10}Zn_{0.90}O$	[0001]	[10-10]	[11-20]	(20±10) nm	-
4	rs	$Mg_{0.80}Zn_{0.2}O$	[111]	[11-2]	[1-10]	(80±20) nm	-
3	wz	$Mg_{0.15}Zn_{0.85}O$	[0001]	[10-10]	[11-20]	(440±80) nm	(515±15) nm
2	rs	$Mg_{0.85}Zn_{0.15}O$	[111]	[11-2]	[1-10]	(135±35) nm	(115±15) nm
1	spinel	$(Mg_{0.65}Zn_{0.35})Al_2O_4$	[111]	[11-2]	[1-10]	(18±6) nm	(20±5) nm
substrate	Al_2O_3	-	[0001]	[2-1-10]	[1-100]		

Table 1 Structure, composition, relative orientation and thickness of the different layers in the $Mg_{0.40}Zn_{0.60}O$-sample and in the $Mg_{0.30}Zn_{0.70}O$ -sample (grey shaded area) after annealing for 1h at 1000°C. The structure and orientation of the layers in the $Mg_{0.30}Zn_{0.70}O$ sample after annealing are identical to those of the first three layers in the $Mg_{0.40}Zn_{0.60}O$-sample. The initial thickness of the $Mg_{0.40}Zn_{0.60}O$ -sample was 700 nm, that of the $Mg_{0.30}Zn_{0.70}O$ -layer was 650 nm.

The scanning TEM (STEM) image of the $Mg_{0.40}Zn_{0.60}O$ layer after annealing depicted in **Figure 5a** reveals thickness fluctuations of the individual layers (cf. **Table 1**). The chemical compositions of the different layers have been determined by STEM- energy dispersive X-ray (EDX) line scan analysis and the resulting composition profile with an accuracy of 5 % is shown in **Fig. 5b** [28]. In the thick wz-$Mg_xZn_{1-x}O$ the ZnO-content is approximately 0.85 just as in the bottom rs-$Mg_xZn_{1-x}O$ layer the Mg-fraction amounts to 0.85, the respective values in the thin top layers are slightly smaller. High resolution STEM images of the interfaces between the different layers of the annealed $Mg_{0.40}Zn_{0.60}O$ sample are provided as supporting information in **Figure S2** [26]. It should be noted that within the different layers the MgO- and ZnO-fractions are constant.

In the $Mg_{0.30}Zn_{0.70}O$ sample only three different layers are formed upon annealing at 1000°C as depicted in the STEM image in **Fig. 5c**: a $(Mg_{0.65}Zn_{0.35})Al_2O_4$ spinel phase interfacing the sapphire substrate, a rs-$Mg_{0.85}Zn_{0.15}O$ –layer, and a wz-$Mg_{0.15}Zn_{0.85}O$ layer as determined by the STEM-EDX line-scan (**Fig. 5d**)**.**

Comparison to **Fig.5a** reveals that the thickness fluctuations of the individual layers after annealing are less pronounced for lower x_0. As no substantial gradients of the Zn- or Mg-concentration are found (**Figs.5b,d**) we conclude that the resulting solid solutions yield the equilibrium concentrations for the respective annealing temperatures. Furthermore, the time scales of the involved diffusion processes are significantly shorter than the applied annealing time.

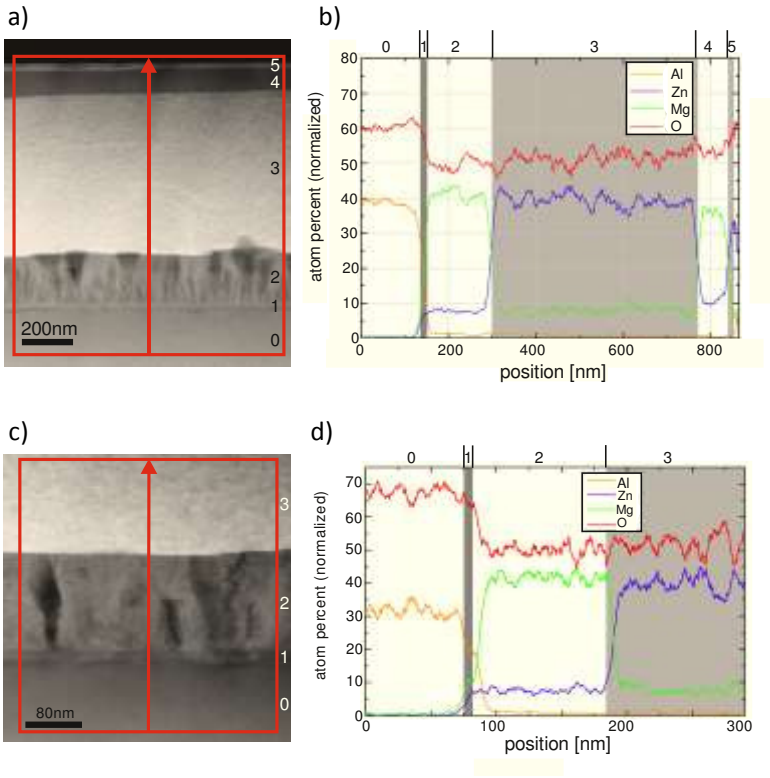

Figure 5 a) STEM image of the $Mg_{0.40}Zn_{0.60}O$ sample after annealing at 1000°C, **b)** EDX line profile for aluminum, zinc, magnesium and oxygen recorded along the red arrow in **a)**, with the frame displaying the averaging area. **c)** STEM image of the $Mg_{0.30}Zn_{0.70}O$ sample after annealing for 1h at 1000°C, **d)** EDX line profile for aluminum, zinc, magnesium and oxygen recorded along the red arrow in **c)**, with the frame displaying the averaging area.

Annealing of the $Mg_{0.05}Zn_{0.95}O$ sample did not result in vertical separation of rs- and wz-phases. Instead, the MgO-concentration in the entire wz-layer remained almost unchanged in agreement with the results of the optical characterization (cf. **Fig. 1**) (supplemental **Fig. S3** [26]). Here, an intermediate $(Mg_{0.35}Zn_{0.65})Al_2O_4$ layer with a textured rather than a single crystalline structure is formed during annealing. Hence, a minimum MgO-concentration is required in the vicinity of the interface to stabilize a single crystalline interfacial spinel layer. This conclusion is further confirmed by the fact that ordered phase separation was not observed for growth of wz-$Mg_xZn_{1-x}O$ layers with $x_0 > 0.3$ on (111) silicon substrates without a MgO/ZnO buffer layer.

We attribute the presence of voids in the rs-$Mg_xZn_{1-x}O$ layer formed during annealing in samples with $x_0 > 0.05$, as visible in **Figs.5a+c**, to the Kirkendall-effect caused by different diffusion properties of metal cations in the Al_2O_3 substrate and the former MgO/ZnO buffer [29] [30].

The effect of the annealing process on the density of threading screw and edge dislocations in the $Mg_{0.40}Zn_{0.60}O$ was analyzed by weak-beam dark-field (WBDF) TEM imaging, as shown in **Fig.6**. Here, edge dislocations were highlighted using the (2-420) reflexes for imaging **(Figs. 6a,b)**, while screw dislocations are made visible in (000-4) WBDF images **(Figs. 6c,d)**. For as-grown layers, the defective MgO/ZnO-buffer layer located between the Al_2O_3-substrate and the as-grown wz-$Mg_xZn_{1-x}O$ -layer is visible with the majority of the defects being annihilated after a few nanometers (**Figs. 6a+c**).

Consistent with earlier reports a higher density of edge-type than screw-type dislocations is observed [8,21,31,32] but no systematic influence of the MgO-concentration is found. Annealing at 1000°C leads to a drastic reduction of the edge and screw dislocation density in the wz-$Mg_xZn_{1-x}O$ layer formed during annealing (**Figs. 6b,d**). The small number of dislocations that is present in the rs-layer close to the interface to the spinel layer does not penetrate the wz-$Mg_xZn_{1-x}O$ layer. This decrease in dislocation density upon annealing is also observed for the layers with x_0 = 0.30 and 0.05 (supplemental **Fig.S4** [26]). As the latter does not show vertical phase separation this result demonstrates that phase separation is not a requirement for the annihilation of threading dislocations during annealing.

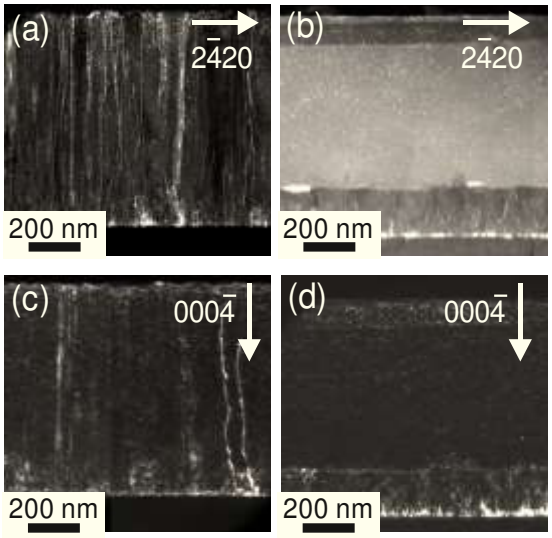

Figure 6 TEM images of the sample with x_0= 0.40 (a) 2-420 WBDF image of the as-grown sample and (b) after annealing for 1 h at 1000°C. (c) 000-4 WBDF image of the as grown sample and (d) after annealing for 1 h at 1000°C.

The improvement of the structural quality is also confirmed by TRPL measurements. While the emission of the as-grown wz-($Mg_{0.30}Zn_{0.70}O$) sample (centered around 3.98 eV) exhibited a non-single-exponential decay and an effective carrier lifetime of (330±20) ps with a weak dependence on x_0, a significantly increased decay time of (800±20) ps and a strict mono-exponential decay was found for the emission of the wz-($Mg_{0.15}Zn_{0.85}O$) layer formed during annealing at 1000°C (supplemental **Fig.S5** [26]). Quantitative evaluation further reveals a strong decrease of disorder contributions and hence a significant improvement of the structural quality of the wz-$Mg_xZn_{1-x}O$ layer formed during annealing [26].

The self-assembled formation of a complex layer structure for the wurtzite $Mg_{0.40}Zn_{0.60}O$ and $Mg_{0.30}Zn_{0.70}O$ layer upon annealing explains the results of the optical and structural analysis. The appearance of the (111) rs-$Mg_xZn_{1-x}O$ diffraction peak in the HRXRD analysis is related to formation of rs-$Mg_xZn_{1-x}O$ layers whereas the optical absorption behavior is dominated by the thick wz-$Mg_xZn_{1-x}O$ layer with reduced Mg-content [32] since the thickness of the wz-$Mg_xZn_{1-x}O$ layer exceeds the absorption length for above band gap excitation and hence the rock salt layers are not visible in absorption or photoluminescence spectroscopy measurements. The increasing peak width in HRXRD analysis after annealing at $T_a \geq 900$°C is attributed to lateral inhomogeneities of the phase separation process.

Corroborated by the results of the TEM analysis these findings prove the transfer of Mg^{2+} from the wz-$Mg_xZn_{1-x}O$ film to the Mg-rich rs-$Mg_xZn_{1-x}O$ films formed during annealing. These observations clearly differ from the mechanisms suggested for thermally activated phase-separation in $Mg_xZn_{1-x}O$ films in refs. [7, 15-18].

Discussion

We assign the evolution of the structural and optical properties revealed in the experimental analysis to a thermally activated phase separation process in the metastable as-deposited wz-$Mg_xZn_{1-x}O$ layer.

In order to independently assess the suggested mechanisms in different states we have investigated the wz-($Mg_{0.30}Zn_{0.70}O$) sample after annealing at different temperatures by PL. As thermally activated processes proceed slower at lower annealing temperatures, the PL spectra recorded after annealing temperatures of 850°C, 900°C and 950°C represent intermediate stages of the phase separation process. As for this sample only three different layers are formed during the annealing process and as, due to the excitation wavelength of 244 nm, PL-emission of the rs-$Mg_xZn_{1-x}O$ layer was not excited, a direct relation between the evolution of the PL spectra from the wz-$Mg_xZn_{1-x}O$ and the evolution of the layer structure can be established and is shown in **Fig.7**.

The weak blue-shift of the optical absorption edge E_{opt} that is observed at low annealing temperatures starting at 800°C for $0.40 \geq x_0 > 0.20$ is assigned to Mg^{2+}-ions moving from interstitial to substitutional lattice sites, in agreement with ref. [7]. This is independently confirmed by the blue-shift in the PL-spectrum in **Fig.7a**. The as-grown film shows a broad emission peak centered at 3.98 eV, referring to an average MgO content of 0.31 [6,8], which is blue-shifted by 75 meV upon annealing at 850°C. In this line the increasing magnitude of this blue-shift of E_{opt} and its decreasing onset temperature with increasing x_0 is attributed to an increasing initial concentration of Mg-interstitials. The red-shift in E_{opt} at higher annealing temperatures $T_a \geq 850$°C is caused by structural changes in the oversaturated wz-$Mg_xZn_{1-x}O$ layer, i.e., the growth of the spinel layer and the formation of rs-$Mg_xZn_{1-x}O$ due to the vertical phase separation process, confirmed by the decreasing onset temperature for vertical phase separation decreases with increasing x_0.

To identify the mechanism responsible for this phase separation process, the (111)-orientation of the Mg-rich rs-$Mg_xZn_{1-x}O$ phase after annealing, which is in contrast to the (001)-orientation observed in other reports [7,15,16], is of importance. This orientation is attributed to the presence of the MgO/ZnO double buffer in the as-grown films and its transformation into a spinel layer upon annealing. In accordance with ref. [19] we cannot identify the spinel layer in as-grown wz-$Mg_{0.4}Zn_{0.6}O$ ($Mg_{0.3}Zn_{0.7}O$) layers. However, a (111)-oriented $(Mg_{0.65}Zn_{0.35})Al_2O_4$ spinel layer with a thickness of (18±6) nm ((20±5)nm) is detected after annealing at 1000°C (layer 1 in **Table 1** and **Figs.3,4**). Hence,

the structural properties of the spinel layer in both samples are almost unaffected by x_0 and are determined by the properties of the buffer layer, strongly suggesting that the phase separation process is initiated at the sapphire/buffer interface. In line with these arguments, the presence of the (111)-oriented spinel surface lowers the free energy of the rs-$Mg_xZn_{1-x}O$ phase at the interface to the oversaturated wz-$Mg_xZn_{1-x}O$ layer and provides a planar seed for the nucleation of rs-$Mg_xZn_{1-x}O$ (layer 2 in **Table 1** and **Fig.3**) by continuation of the fcc O^{2-}-sublattice and incorporation of mobile metal cations on octahedral lattice sites. Hence, demixing and phase separation relies on nucleation. As homogeneous nucleation within a solid phase is energetically unfavorable, heterogeneous nucleation at a phase boundary is the starting point of phase separation in the present case. Note that this phase separation involves different crystal structures and hence a continuous dependence of the free energy on the MgO-(ZnO)-concentration, being expected for a solid solution with complete miscibility, cannot be established. The MgO-concentration in the rs-$Mg_xZn_{1-x}O$ is determined by the equilibrium composition for the respective annealing temperature, x_{rs}. The latter is found to be $(Mg_{0.85}Zn_{0.15})O$ for an annealing temperature of 1000°C by TEM-EDX for x_0 = 0.3 and x_0 = 0.4 (schematically shown in **Fig.7b**). After nucleation, growth of the rs-$(Mg_{0.85}Zn_{0.15})O$ proceeds, similar to the mechanism of precipitate growth with a planar interface [34].

Due to the higher MgO concentration in the rs-layer, Mg^{2+}-ions are depleted in the adjacent region of the wz-$Mg_xZn_{1-x}O$ layer, causing downhill diffusion of Mg^{2+}-ions from the wz-$Mg_xZn_{1-x}O$ to the interface[1] and a displacement of the rs-/wz-interface into the wz-$Mg_xZn_{1-x}O$ layer. The related decrease of the MgO-concentration in the wz-$Mg_xZn_{1-x}O$ layer results in a red-shift of E_{opt} and of the respective PL emission peak, as depicted in **Fig.7b**. Increasing T_a to 900°C results in a red shift of the PL emission energy to 3.92 eV, i.e. a decrease of the average Mg-fraction in the wz-$Mg_xZn_{1-x}O$ layer to 0.28 [6,8]. For T_a = 950°C a second emission peak centered around 3.80 eV emerges. It corresponds to a Mg-fraction x of 0.21 [8] and indicates the ongoing depletion of Mg^{2+} in the wz-(Zn,Mg)O layer due to transfer to the rs-layer. The presence of lateral inhomogeneities of the phase separation

[1] The net diffusion of Mg^{2+} from the wz-$Mg_xZn_{1-x}O$ layer towards the rs-$(Mg_{0.85}Zn_{0.15})O$ layer implies the diffusion of Zn^{2+} into the opposite direction.

process on the length scale of the spot size for excitation (2 mm²) can also contribute to the simultaneous appearance of two emission peaks.

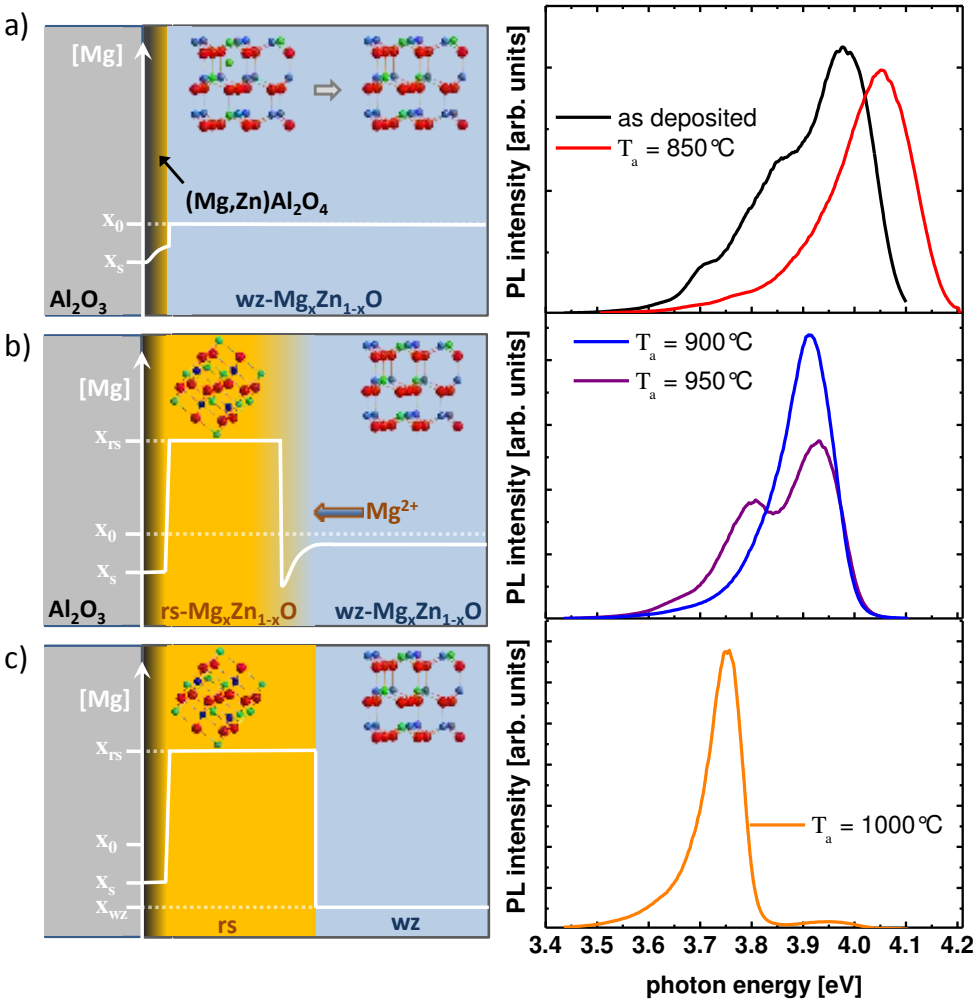

Figure 7 Evolution of the phase separation epitaxy process with annealing temperature and related PL spectra of the wz-$Zn_{0.7}Mg_{0.3}O$ sample (measured at T = 10 K). The right panel shows a schematic overview of the layer structure and of the Mg-profile (white axis and lines). (a) After annealing at low annealing temperatures (T_a = 850°C); b) after annealing at moderate temperatures (T_a = 850°C, 900°C); c) after annealing at 1000°C. Details are given in the text.

The growth of the rs-$Mg_xZn_{1-x}O$ layer is self-limiting and proceeds until the Mg-fraction in the remaining wz-$Mg_xZn_{1-x}O$ reaches the equilibrium value for the respective annealing temperature, x_{wz} (cf. **Fig.7c**), which is determined to values between 0.15 and 0.18 by optical absorption and TEM-EDX analysis in accordance with refs. [15, 16]. This is corroborated by the dominance of only one PL emission peak at 3.75 eV, corresponding to a MgO-content of 18 % (**Fig.7c**) [8]. Accordingly, an increase in x_0 results in an increased thickness of the rs-$Mg_xZn_{1-x}O$ formed during annealing, as more

Mg is consumed before the content in the remaining layer reaches x_{wz}. Further, the Mg-fractions x_{rs} and x_{wz} of the different layers formed during the phase separation process represent the respective equilibrium concentrations and do not depend on x_0. Both conclusions are in agreement with the experimental results. In contrast, the latter quantities are likely to depend on T_a and from the data presented in **Fig.1, Fig.5 and Fig.7** it cannot be excluded that for higher annealing temperatures the saturation concentration of 4% MgO in wz-$Mg_xZn_{1-x}O$ reported in ref. [11] is achieved.

For high values of x_0, i.e. for the wz-$Mg_{0.4}Zn_{0.6}O$ film, the generation of the wz-phase with Mg-fraction x_{wz} upon annealing results in the accumulation of Mg^{2+} on the top surface of wz-layer. We assume that the presence of this Mg-rich region initiates the formation of the second epitaxial rs-/wz-$Mg_xZn_{1-x}O$ double layer with smaller layer thickness. As this process is related with uphill diffusion of the Mg^{2+} -and Zn^{2+} - ions this process is similar to spinodal decomposition observed in other compound semiconductors [35-37], although it describes the demixing into two phases with a different crystal structure. However, this process, which should also be observable for thick initial wz-$Mg_xZn_{1-x}O$ layers, needs further investigation.

The vertical phase separation process results in the formation of self-assembled epitaxial rs-/wz-$Mg_xZn_{1-x}O$ heterostructures and the formation of natural interfaces between layers with different crystal structures (**Fig. S2** [26]). As these interfaces are formed during the annealing process, i.e. in a state of high ion mobility, strain accumulation due to lattice mismatch is reduced by interfacial relaxation. The decreasing interface coherence results in a reduced dislocation density. This latter process is mainly facilitated by the ion mobility and does not depend on the phase separation as evidenced in **Fig.S4** [26] for the wz-($Mg_{0.05}Zn_{0.95}$) layer. Furthermore, the formation of the rs-$Mg_xZn_{1-x}O$ epitaxial layer also reduces the lattice mismatch between the spinel and the wurtzite phase (3.5% for (Mg,Zn)Al_2O_4/rs-($Mg_{0.85}Zn_{0.15}$)O instead of 13% for (Mg,Zn)Al_2O_4/wz-($Zn_{0.6}Mg_{0.4}O$)) [14,19].

Conclusion

We have demonstrated the self-assembly of epitaxial rs-$Mg_xZn_{1-x}O$/wz-$Mg_xZn_{1-x}O$ heterostructures by thermally activated vertical phase separation in wz-($Mg_xZn_{1-x}O$) layers with $x \geq 0.30$ grown by PAMBE on c-plane sapphire substrates. This process, which is accompanied by a drastic decrease in edge- and screw-dislocation density, is initiated by the formation of a (111)-oriented spinel $(Mg,Zn)Al_2O_4$ layer due to interdiffusion of Al^{3+} and Mg^{2+} from the substrate and the MgO buffer layer, that acts as a planar seed for the precipitation of an *rs*-$Mg_xZn_{1-x}O$ film with an equilibrium Mg-fraction of $x_{rs} = 0.85$ at an annealing temperature of 1000°C by *phase separation epitaxy.* This self-limiting growth process proceeds until the Mg-fraction in the remaining wz-layer reaches its equilibrium value of 0.15.

During this process self-assembled heterointerfaces between rs- and wz-$Mg_xZn_{1-x}O$ layers are formed and the wz-$Mg_xZn_{1-x}O$ layers after annealing exhibit larger quantum yield, longer carrier lifetimes, and less disorder compared to the initially deposited film.

Thus, starting from a highly dislocated Mg-oversaturated wz-$Mg_xZn_{1-x}O$ layer on c-plane sapphire substrate the epitaxial formation of rs- and wz-$Mg_xZn_{1-x}O$ films with extremely low density of extended defects and thermally stable composition is possible. The *phase separation epitaxy* process described here provides a straight-forward technique for preparation of wz- and rs-templates for quasi-homoepitaxial growth which could also be transferred to $Mg_xZn_{1-x}O$ layers fabricated by other deposition techniques.

Acknowledgements

Authors from JLU Giessen acknowledge support within the LOEWE program of excellence of the Federal State of Hessen (project initiative STORE-E) and by the LaMa of JLU. Authors from Marburg acknowledge support from the Deutsche Forschungsgemeinschaft (DFG) within the collaborative research center SFB 1083 "Structure and Dynamics of Internal Interfaces.

References

[1] D. C. Look, Mat. Sci. Eng. B **80**, 383 (2001).

[2] D. G. Thomas, J. Phys. Chem. Solids **15**, 86 (1960).

[3] H. D. Sun, T. Makino, Y. Segawa, M. Kawasaki, A. Ohtomo, K. Tamura, and H. Koinuma, J. Appl. Phys. **91**, 1993 (2002).

[4] Th. Gruber, C. Kirchner, R. Kling, F. Reuss and A. Waag, Appl. Phys. Lett. **84**, 5359 (2004).

[5] B. Laumer, T. A. Wassner, F. Schuster, M. Stutzmann, M. Rohnke, A. Chernikov, V. Bornwasser, M. Koch, S. Chatterjee, M. Eickhoff, J. Appl. Phys. **110**, 093513 (2011).

[6] A. Ohtomo, M. Kawasaki, T. Koida, K. Masubuchi, H. Koinuma, Y. Sakurai, Y. Yoshida, T. Yasuda, and Y. Segawa, Appl. Phys. Lett. **72**, 2466 (1998).

[7] D.Y. Jiang, D. Z. Shen, K. W. Liu, C. X. Shan, Y. M. Zhao, T. Yang, B. Yao, Y. M. Lu, and J. Y. Zhang, Semicond. Sci. Technol. **23**, 035002 (2008).

[8] T. A. Wassner, B. Laumer, S. Maier, A. Laufer, B. K. Meyer, M. Stutzmann, and M. Eickhoff, J. Appl. Phys. **105**, 023505 (2009).

[9] R. D. Shannon, Acta Crystallogr. A **32**, 751 (1976).

[10] S. Limpijumnong and W. R. L. Lambrecht, Phys. Rev. B **63**, 104103 (2001).

[11] E. R. Segnit, A. E. Holland, J. Am. Cer. Soc. **48**, 409 (1965).

[12] S. Fujita, T. Takagi, H. Tanaka, and S. Fujita, phys. stat. sol. B **241**, 599 (2004).

[13] W. I. Park, G.-C. Yi, and H. M. Jang, Appl. Phys. Lett. **79**, 2022 (2001).

[14] Z. Vashaei, T. Minegishi, H. Suzuki, T. Hanada, M. W. Cho, T. Yao, A. Setiawan, J. Appl. Phys. **98**, 054911 (2005).

[15] W. Liu, S. Gu, S. Zhu, J. Ye, F. Qin, S. Liu, X. Zhou, L. Hu, R. Zhang, Y. Shi, Y. Zheng, J. Cryst. Growth **277**, 416 (2005).

[16] A. Ohtomo, R. Shiroki, I. Ohkubo, H. Koinuma, and M. Kawasaki, Appl. Phys. Lett. **75**, 4088 (1999).

[17] H. Li, Y. Zhang, X. Pan, T. Wang, E. Xie, J. All. Comp. **472**, 208 (2009).

[18] Z. G. Ju, C. X. Shan, C. L. Yang, J. Y. Zhang, B. Yao, D. X. Zhao, D. Z. Shen, X. W. Fa, Appl. Phys. Lett. **94**, 101902 (2009).

[19] A. Bakin, J. Kioseoglou, B. Pecz, A. El-Shaer, A.-C. Mofor, J. Stoemenos, A. Waag, J. Cryst. Growth **208**, 314 (2007).

[20] Due to the low deposition temperature and the high MgO-concentration a broad absorption peak was observed for samples with $x_0 \geq 0.20$. Hence, determination of the absorption edge by consideration of exciton-phonon complexes as demonstrated in [25] was not possible for all samples. Furthermore, lateral fluctuations of the MgO-content of up to ± 0.02 were observed. The Mg-fractions in the as-deposited reference samples, determined according to refs [6, 8] were 0.054, 0.11, 0.22, 0.29, 0.38. As different parts of the same sample were used for the annealing experiments we restrict the precision in the MgO-content to 0.05, 0.10, 0.20, 0.30, and 0.40 following the arguments above.

[21] T. A. Wassner, B. Laumer, M. Althammer, S.T.B. Gönnenwein, M. Stutzmann, M. Eickhoff, M.S. Brandt, Appl. Phys. Lett. **97**, 092102 (2010).

[22] Y. A. Osipiyan, I. S. Smirnova, phys. stat. sol. (b) **30**, 19 (1968).

[23] D. J. H. Cockayne, I. L. F. Ray, M. J. Whelan, Philosophical Magazine **20**, 1265 (1969).

[24] A. Howie, C. H. Sworn, Philosophical Magazine **22**, 861 (1970).

[25] M. D. Neumann, C. Cobet, N. Esser, B. Laumer, T. A. Wassner, M. Eickhoff, M. Feneberg, and R. Goldhahn, J. Appl. Phys. **110**, 013520 (2011).

[26] See supplemental material at [URL will be inserted by AIP] for additional experimental results.

[27] P. Stadelmann, Ultramicroscopy **21**, 131 (1987).

[28] In addition to lateral inhomogeneities of the phase separation process also rs-MgO precipitates with diameters > 100 nm and different orientation ((001), (111)) with respect to the sapphire substrates were found in some cases. We attribute the presence of such inclusions to inhomogeneities in the MgO-concentration of the as-grown sample.

[29] H. J. Fan, M. Knez, R. Scholz, D. Hesse, K. Nielsch, M. Zacharias, U. Gösele, Nano Lett. **7**, 993 (2007).

[30] A.D. Smigelskas, E.O. Kirkendall, Trans. AIME **171**, 130 (1947).

[31] K. Miyamoto, M. Sano, H. Kato, T. Yao, J. Cryst Growth **265**, 34 (2004).

[32] A. Setiawan, H. J. Ko, S. K. Hong, Y. Chen, T. Yao, Thin Solid Films **445**, 213 (2003).

[33] We assign the presence of (002) rs-$Mg_xZn_{1-x}O$ diffraction peak in the HRXRD analysis to MgO precipitates that have been observed.

[34] D.A. Porter, K. E. Eastering, Phase Transformations in Metals and Alloys, 1st Edition (1981), Chapman and Hall, London.

[35] J. W. Cahn, J. E. Hilliard, J. Chem. Phys. **31**, 688 (1959).

[36] G. B. Stringfellow, J. Cryst. Growth 65, **454** (1983).

[37] I. P. Ipatova, V. G. Malyshkin, V. A. Shchukin, J. Appl. Phys. **74**, 7198 (1993).